Structure and Electrical Properties of Unsubstituted Oligothiophenes End-Capped at the β-Position

Jiro Chisaka,[†,‡] Ming Lu,[‡,||] Shuichi Nagamatsu,[‡,⊥] Masayuki Chikamatsu,[‡] Yuji Yoshida,*[,‡] Midori Goto,[§] Reiko Azumi,*[,‡] Masafumi Yamashita,[†] and Kiyoshi Yase[‡]

Department of Physics, Tokyo University of Science, 2641 Yamazaki, Noda, Chiba 278-8510, Japan, Photonics Research Institute, National Institute of Advanced Industrial Science and Technology (AIST), Tsukuba Central 5, 1-1-1 Higashi, Tsukuba, Ibaraki 305-8565, Japan, Technical Center, National Institute of Advanced Industrial Science and Technology (AIST), Tsukuba Central 5, 1-1-1 Higashi, Tsukuba, Ibaraki 305-8565, Japan, Department of Chemistry, Harbin Normal University, Harbin 150080, China, and Department of Computer Science and Electronics, Kyushu Institute of Technology, 680-4 Kawazu, Iizuka, Fukuoka 820-8502, Japan

Received January 18, 2007. Revised Manuscript Received March 13, 2007

The relationship between molecular structure, molecular packing in bulk, film structure, and electrical characteristics were investigated for the unsubstituted oligothiophene pentamer and hexamer, both of which have terminal thiophene units linking at the β-position (β*n*T; $n = 5, 6$). To reveal the molecular geometry and molecular packing of β*n*Ts, X-ray single-crystal analysis was carried out. For the electrical characterization, organic field-effect transistors (OFETs) based on the β*n*T thin films were fabricated at various substrate temperatures. Film structure was investigated by X-ray diffraction and atomic force microscopy. Highest field-effect mobility of OFET was 0.050 $cm^2\ V^{-1}\ s^{-1}$ for β6T at a substrate temperature of 120 °C and 0.020 $cm^2\ V^{-1}\ s^{-1}$ for β5T at a substrate temperature of 90 °C, which are slightly smaller than those of α-oligothiophene isomers with the same number of thiophene rings. β6T OFET characteristics depend on the film morphology such as grain size, while the dependence of β5T OFET on the morphology is slight. The different behavior of β6T and β5T can be interpreted by their different molecular orientation with respect to the film surface.

Introduction

Organic thin film devices have been actively investigated for the past several decades in anticipation of fascinating characteristics of organic materials such as being lightweight and having flexibility and excellent processability. Several organic devices such as organic photoconductors, liquid crystal displays, and organic electroluminescent (EL) devices have already been used on a commercial basis. Research studies aiming at practical device application have also started for organic transistors.

Basic characteristics of organic field-effect transistors (OFETs) out of organic semiconductor thin films have been investigated since the 1980s.[1,2] Recently, OFETs with their mobility approaching that of polysilicon and amorphous silicon have been reported.[3] Moreover, integrated circuits and active matrix displays using OFETs have been reported.[4,5] However, many problems in performance and durability are still left unsolved.

To put the OFETs development into the more practical phase, approaches from several viewpoints are indispensable: (1) development of new materials with high performance, (2) device design, and (3) processing technology. Materials development includes not only the syntheses of new compounds but also control of molecular packing and orientation because the performance of organic compounds in thin films originates from the solid state where the molecules are packed in a certain manner. A detailed understanding is needed for the relationship between various factors such as structure (chemical structure, molecular packing, structure of thin films, and so on) and physical properties.

Oligothiophenes are promising materials for OFET because of their high mobility, chemical stability, and ease of chemical modification.[6] Various substituted oligothiophenes have been newly synthesized and applied to OFETs. Garnier et al. improved solubility as well as hole mobility of sexithiophene by introducing two hexyl groups at both edges of the molecule (5,5′′′′′-dihexyl-α-sexithiophene, DH6T).[7]

* To whom correspondence should be addressed. Phone: +81-29-861-6252. Fax: +81-29-861-6303. E-mail: yuji.yoshida@aist.go.jp; reiko.azumi@aist.go.jp.

† Tokyo University of Science.

‡ Photonics Research Institute, National Institute of Advanced Industrial Science and Technology.

§ Technical Center, National Institute of Advanced Industrial Science and Technology.

|| Harbin Normal University.

⊥ Kyushu Institute of Technology.

(1) Kudo, K.; Yamashina, M.; Morizumi, T. *Jpn. J. Appl. Phys.* **1984**, *23*, 130.

(2) Tsumura, A.; Koezuka, H.; Ando, T. *Appl. Phys. Lett.* **1986**, *49*, 1210.

(3) Dimitrakopoulos, C. D.; Malenfant, P. R. L. *Adv. Mater.* **2002**, *14*, 99.

(4) Gelinck, G. H.; Genus, T. C. T.; de Leeuw, D. M. *Appl. Phys. Lett.* **2000**, *77*, 1487.

(5) Huitema, H. E. A.; Gelinck, G. H.; van der Putten, J. B. P. H.; Kuijk, K. E.; Hart, C. M.; Cantatore, E.; Herwig, P. T.; van Breemen, A. J. J. M.; de Leeuw, D. M. *Nature* **2001**, *414*, 599.

(6) Fichou, D., Ed. *Handbook of Oligo- and Polythiophenes*; Wiley-VCH: New York, 1999.

10.1021/cm0701658 CCC: $37.00
Published on Web 04/19/2007

Letizia et al. reported an n-type oligothiophene derivative by introducing fluorinated substituents.[8] Kunugi et al. reported a solution-processable ambipolar OFET based on fullerene (C60)-attached oligothiophene.[9] Videlott-Ackermann et al. reported the improvement of device durability by employing a styryl unit as a terminal substituent.[10]

Unsubstituted α-oligothiophenes, the simplest compounds among numerous thiophene-based derivatives, have been intensively studied[11−26] since Horowitz et al. demonstrated high hole mobility of α-sexithiophene.[11] Until now, many investigations have been reported such as X-ray single-crystal structure analyses,[12−18] structure-physical properties relationship of thin films including the effect of oligomerization degree,[19−22] and dependence on the fabrication process such as substrate temperature and evaporation rate.[21−26] These results provide rich insights into structure-physical properties relationship of thiophene-based materials.

In our previous work, we investigated the correlation between the parity of ring number, crystal structure, and OFET characteristics of unsubstituted α-oligothiophenes.[17,22] In single crystals, quinquethiophene (α-5T) and septithiophene (α-7T) tend to pack in the less ordered manner compared to the oligomers with even number of thiophene rings. The evaporated thin films of α-5T and α-7T fabricated at relatively low substrate temperature contain two polymorphs coexisting. The charge mobility of such films is relatively low, indicating that the lack of order in molecular packing affects, though indirectly, the FET performance of the thin film.

Scheme 1. Chemical Structure and Synthetic Scheme of *βn*Ts

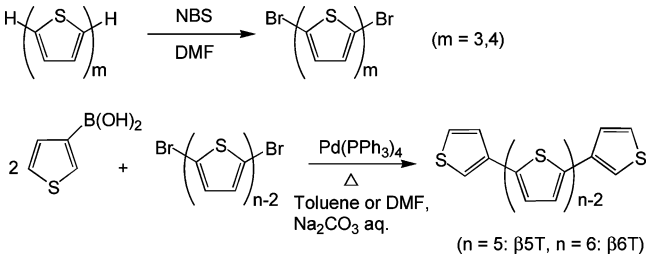

In this work, we have synthesized a hexamer and a pentamer of unsubstituted oligothiophene with both the terminal thiophene rings linking at the *β*-position, i.e., structural isomers of unsubstituted α-oligothiophenes (Scheme 1, here abbreviated as *βn*Ts, where *n* represents the number of thiophene rings in a molecule). Due to the change of the linking site, the orientation of sulfur and carbon atoms at the outermost thiophene rings is different from the case of α-oligothiophenes, which will affect their molecular packing, and consequently, the physical properties such as charge mobility. Using this new series of compounds, we have investigated in detail the structure-physical properties relationship concerning OFET performance.

Experimental Section

Materials. 2,2′:5′,2″:5″,2‴-Quaterthiophene, 2,2′:5′,2″-terthiophene, 3-thiopheneboronic acid, and tetrakis(triphenylphosphine)palladium(0) were purchased from Aldrich and used without further purification. Other chemicals were purchased from Wako Chemicals Co. and used as received. 5,5‴-Dibromo-2,2′:5′,2″:5″,2‴-quaterthiophene and 5,5”-dibromo-2,2′:5′,2″-terthiophene was synthesized following the literature.[27]

Synthesis of 3,2′:5′,2″:5″,2‴:5‴,2⁗:5⁗,3⁗⁗-Sexithiophene (*β*6T). The synthetic scheme of the compound is shown in Scheme 1. To 75 mL of dimethylformamide (DMF) in a three-necked flask were added 0.28 g (2.2 mmol) of 3-thiopheneboronic acid, 0.49 g (1.0 mmol) of 5,5‴-dibromo-2,2′:5′,2″:5″,2‴-quaterthiophene, and 0.12 g (0.10 mmol) of tetrakis(triphenylphosphine)palladium(0). After 10 min of nitrogen bubbling, 0.55 g (5.2 mmol) of Na_2CO_3 in 3 mL of H_2O was added. The mixed solution was refluxed for 2.5 h. The brown precipitate was filtered and washed with pure water. The crude product was sublimed twice to give 0.12 g (0.24 mmol) of orange crystals. Yield: 24%. mp: 346−348 °C. Elemental analysis: Calcd for $C_{24}H_{14}S_6$: C, 58.26; H, 2.85; S, 38.89%. Found: C, 58.50; H, 2.72; S, 38.88%.

Synthesis of 3,2′:5′,2″:5″,2‴:5‴,3⁗-Quinquethiophene (*β*5T). The synthetic scheme of the compound is shown in Scheme 1. To 80 mL of DMF in a three-necked flask were added 0.78 g (6.1 mmol) of 3-thiopheneboronic acid, 1.0 g (2.5 mmol) of 5,5″-dibromo-2,2′:5′,2″-terthiophene, and 0.29 g (0.25 mmol) of tetrakis-(triphenylphosphine)palladium(0). After 10 min of nitrogen bubbling, 1.0 g (9.4 mmol) of Na_2CO_3 in 3 mL of H_2O was added. The mixed solution was refluxed for 7.5 h. The precipitate was filtered and washed with pure water. The crude product was sublimed twice to give 0.28 g (0.69 mmol) of yellowish-orange crystals. Yield: 27%. mp: 312−314 °C. Elemental analysis: Calcd for $C_{20}H_{12}S_5$: C, 58.22; H, 2.93; S, 38.85%. Found: C, 58.54; H, 2.75; S, 38.26%.

(7) Garnier, F.; Yassar, A.; Hajlaoui, R.; Horowitz, G.; Deloffre, F.; Servet, B.; Ries, S.; Alnot, P. *J. Am. Chem. Soc.* **1993**, *115*, 8716.
(8) Letizia, J. A.; Facchetti, A.; Stern, C. L.; Ratner, M. A.; Marks, T. J. *J. Am. Chem. Soc.* **2005**, *127*, 13476.
(9) Kunugi, Y.; Takimiya, K.; Negishi, N.; Otsubo, T.; Aso, Y. *J. Mater. Chem.* **2004**, *14*, 2840.
(10) Videlot-Ackermann, C.; Ackermann, J.; Brisset, H.; Kawamura, K.; Yoshimoto, N.; Raynal, P.; El Kassmi, A.; Fages, F. *J. Am. Chem. Soc.* **2005**, *127*, 16346.
(11) Horowitz, G.; Fichou, D.; Peng, X. Z.; Xu, Z.; Garnier, F. *Solid State Commun.* **1989**, *72*, 381.
(12) Fichou, D. *J. Mater. Chem.* **2000**, *10*, 571.
(13) Siegrist, T.; Kloc, C.; Laudise, R. A.; Katz, H. E.; Haddon, R. C. *Adv. Mater.* **1998**, *10*, 379.
(14) Antolini, L.; Horowitz, G.; Kouki, F.; Garnier, F. *Adv. Mater.* **1998**, *10*, 382.
(15) Horowitz, G.; Bachet, B.; Yassar, A.; Lang, P.; Demanze, F.; Fave, J.-L.; Garnier, F. *Chem. Mater.* **1995**, *7*, 1337.
(16) Siegrist, T.; Fleming, R. M.; Haddon, R. C.; Laudise, R. A.; Lovinger, A. J.; Katz, H. E.; Bridenbaugh, P.; Davis, D. D. *J. Mater. Res.* **1995**, *10*, 2170.
(17) Azumi, R.; Goto, M.; Honda, K.; Matsumoto, M. *Bull. Chem. Soc. Jpn.* **2003**, *76*, 1561.
(18) Fichou, D.; Bachet, B.; Demanze, F.; Billy, I.; Horowitz, G.; Garnier, F. *Adv. Mater.* **1996**, *8*, 500.
(19) Hajlaoui, R.; Horowitz, G.; Garnier, F.; Arce-Brouchet, A.; Laigre, L.; El Kassmi, A.; Demanze, F.; Kouki, F. *Adv. Mater.* **1997**, *9*, 389.
(20) Horowitz, G.; Hajlaoui, R.; Fichou, D.; El Kassmi, A. *J. Appl. Phys.* **1999**, *85*, 3202.
(21) Horowitz, G.; Hajlaoui, M. E. *Adv. Mater.* **2000**, *12*, 1046.
(22) Nagamatsu, S.; Kaneto, K.; Azumi, R.; Matsumoto, M.; Yoshida, Y.; Yase, K. *J. Phys. Chem. B* **2005**, *109*, 9374.
(23) Servet, B.; Horowitz, G.; Ries, S.; Lagorsse, O.; Alnot, P.; Yassar, A.; Deloffre, F.; Srivastava, P.; Hajlaoui, R.; Lang, P.; Garnier, F. *Chem. Mater.* **1994**, *6*, 1809.
(24) Hajlaoui, M. E.; Garnier, F.; Hassine, L.; Kouki, F.; Bouchriha, H. *Synth. Met.* **2002**, *129*, 215.
(25) Biscarini, F.; Zamboni, R.; Samorí, P.; Ostoja, P.; Taliani, C. *Phys. Rev. B* **1995**, *52*, 14868.
(26) Melucci, M.; Gazzano, M.; Barbarella, G.; Cavallini, M.; Biscarini, F.; Maccagnani, P.; Ostoja, P. *J. Am. Chem. Soc.* **2003**, *125*, 10266.
(27) Bäuerle, P.; Würthner, F.; Götz, G.; Effenberger, F. *Synthesis* **1993**, 1099.

Table 1. Structure Determination Summary

	β6T	β5T
formula	$C_{24}H_{14}S_6$	$C_{20}H_{12}S_5$
fw	494.77	412.65
temp [K]	183(2)	203(2)
cryst syst	monoclinic	monoclinic
space group	*P*2(1)/*c*	*P*2(1)/*c*
a [Å]	22.447(2)	7.6053(5)
b [Å]	7.7159(7)	41.913(3)
c [Å]	5.9918(6)	11.0306(7)
α [deg]	90	90
β [deg]	91.434(2)	90.078(1)
γ [deg]	90	90
V [Å^3]	1037.4(2)	3516.1(4)
Z	2	8
ρ_{calcd} [Mg m^{-3}]	1.584	1.559

X-ray Single-Crystal Analysis. Large enough single crystals were obtained by subliming the crude compounds using the glassware previously reported.[17] Diffraction data were collected on a Bruker Smart Apex diffractometer with Mo Kα radiation. The data reduction was carried out with SAINTPLUS V6.22.[28] Semiempirical absorption correction was applied with SADABS.[29] The structure determination was done with direct methods and refinements with full-matrix least-squares on F^2 with SHELXTL Version 6.12.[30] Hydrogen atoms were added using the riding model with the isotropic displacement parameters 1.2-fold of the equivalent U_{ij} of the corresponding carbon atoms. The graphics were performed using PLATON.[31]

Band Structure Calculation. The band calculation was carried out using the program and the parameter reported by Mori et al.[32] The procedure to approximate the band structures is as shown below:[33,34]

(1) The molecular orbitals of a single molecule were calculated by extended Hückel method using the molecular geometry obtained by X-ray single-crystal analyses.

(2) As a p-type organic semiconductor, the intermolecular overlap (*S*) was calculated at the highest occupied molecular orbital (HOMO) level.

(3) Transfer integrals (*t*) were estimated using the equation $t = ES$, where *E* is the HOMO energy level. This equation is same as that generally used in the extended Hückel method to obtain resonance integrals. A constant value of $E = -10$ eV was employed for both β6T and β5T because the HOMO energies estimated for the two compounds deviate only slightly from each other.

(4) With use of the standard tight-binding approximation, the band structure of the HOMO was calculated.

Since the interest of charge transport is focused on the directions perpendicular to the long molecular axis, the band calculation was carried out along the reciprocal lattice vectors of the shortest and the second shortest crystallographic axes.

(28) Bruker, *SMART* (Version 5.625) and *SAINTPLUS* (Version 6.22); Bruker Axs Inc.: Madison, WI, 2000.
(29) Sheldrick, G. M. *SHELXTL*, Version 6.12; Bruker AXS: Madison, WI, 2000.
(30) Sheldrick, G. M. *SADABS*; University of Göttingen: Göttingen, Germany, 1996.
(31) Spek, A. *Acta Crystallogr. A* **1990**, *46*, C34.
(32) Mori, T.; Kobayashi, A.; Sasaki, Y.; Kobayashi, H.; Saito, G.; Inokuchi, H. *Bull. Chem. Soc. Jpn.* **1984**, *57*, 627.
(33) To ensure our calculation procedure, we also calculated the band structure of the HOMO of the α-6T high-temperature polymorph and compared the results with those of Haddon et al.[34] The shape of the HOMO band was similar to their results while the energy level and the bandwidth were different. The qualitative discrepancies may be due to the difference in the calculation program and parameters.
(34) Haddon, R. C.; Siegrist, T.; Fleming, R. M.; Bridenbaugh, P. M.; Laudise, R. A. *J. Mater. Chem.* **1995**, *5*, 1719.

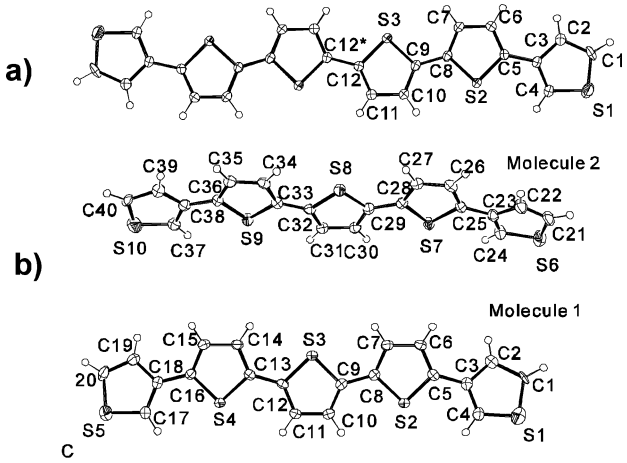

Figure 1. Molecular structures of βnTs with atomic numbering scheme. Displacement ellipsoids are drawn at the 50% probability level. (a) β6T; (b) β5T. There are two crystallographically independent molecules in a unit cell of β5T.

Film Preparation. Oligothiophene films were deposited on a substrate surface by thermal evaporation at a base pressure of 10^{-6} Torr and a deposition rate of ca. 0.03 nm s^{-1}. During the evaporation, the substrate was held at controlled temperatures (β5T: 25, 50, 90, and 130 °C; β6T: 25, 120, and 180 °C). The resulting film thickness was approximately 100 nm.

Thin Film Characterization. The structure of deposited oligothiophene films was investigated by X-ray diffraction (XRD) analysis which was carried out on a Rigaku RU-300 using $2\theta-\theta$ scan method with focused Cu Kα radiation. The film morphology was investigated by atomic force microscopy (AFM), which was carried out on a Molecular Imaging equipped with a NanoScope IIIa controller using the contact mode.

Device Fabrication and Characterization. Top contact type OFETs were constructed on highly doped n-type silicon wafers covered with 300 nm thick silicon dioxide with a capacitance per unit area (C_{ins}) of 10 nF cm^{-2}. Prior to the deposition of oligothiophenes, the surface of the silicon dioxide was treated with 1,1,1,3,3,3-hexamethyldisilazane. The oligothiophenes were deposited on the treated substrate surfaces under the above-mentioned conditions. To complete the devices, we evaporated gold source-drain electrodes on top of the oligothiophene films through a shadow mask, defining the channel length of $L = 20$ μm and channel width of $W = 5$ mm. The OFET devices were characterized using computer-controlled two-source measure units (Keithley 6430 and 2400 sourcemeters) under vacuum ($<10^{-6}$ Torr) at room temperature. The mobility (μ) and the threshold voltage (V_T) were calculated in a saturation regime (drain voltage is $V_D = -50$ V) using the equation $I_D = (WC_{ins}/2L)\mu(V_G - V_T)$,[2] where I_D is the source-drain current and V_G is the gate voltage.

Results and Discussion

X-ray Single-Crystal Analysis. Both β6T and β5T formed large enough single crystals for X-ray analysis by sublimation using the apparatus described earlier.[17] The structural data are summarized in Table 1. The molecular geometry of β6T with atomic numbering scheme is shown in Figure 1a. The molecules exhibit flat orientation with relatively small dihedral angles between the neighboring thiophene rings. The dihedral angle at the outermost position is larger than those of inner ones. The majority of sulfur atoms at the terminal thiophene rings face the same direction (syn conformation) as the sulfur atoms of their neighboring

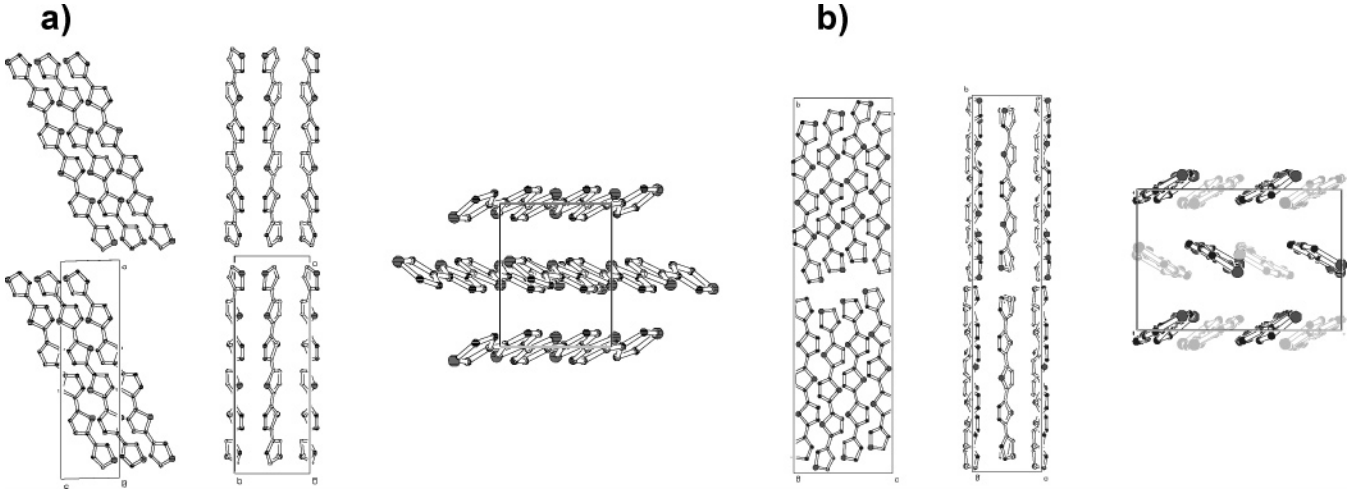

Figure 2. Packing diagrams of βnTs viewed from three crystallographic axes. (a) β6T; (b) β5T.

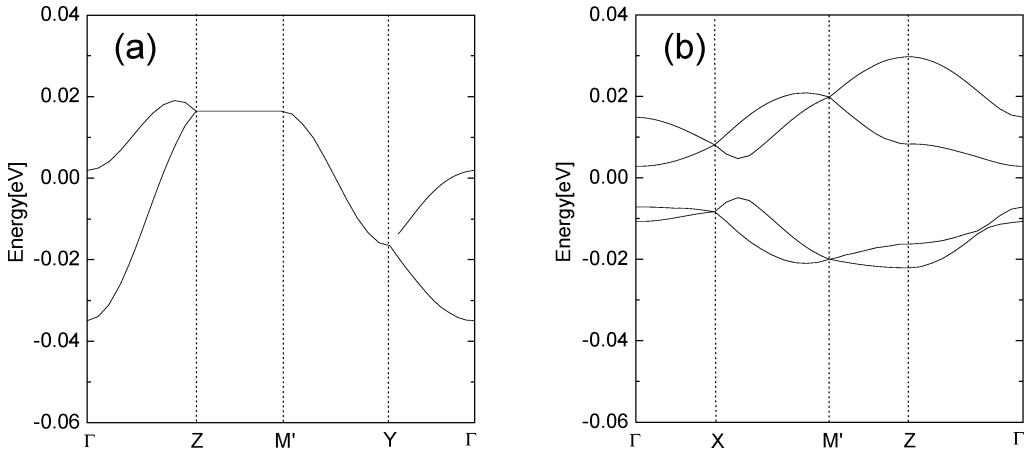

Figure 3. HOMO band structure of oligothiophenes calculated by transfer integrals: (a) β6T: $\Gamma = (0, 0, 0)$, $Z = (0, 0, \pi/c)$, $M' = (0, \pi/b, \pi/c)$, and $Y = (0, \pi/b, 0)$. (b) β5T: $\Gamma = (0, 0, 0)$, $X = (\pi/a, 0, 0)$, $M' = (\pi/a, 0, \pi/c)$, and $Z = (0, 0, \pi/c)$.

inner thiophene rings, although a small disorder of syn and anti conformation was suggested (small portion of S1 locates at C1 position). The molecule possesses the center of symmetry at the middle of the molecule.

Figure 1b shows the molecular geometry of β5T. There are two crystallographically independent molecules in an asymmetric unit whose conformations do not deviate much from each other. The feature of the molecular conformation is similar to that of β6T, except for the lack of center of symmetry.

Figure 2a shows the packing diagram of β6T. The molecules are packed into herringbone structure, which is also commonly observed for unsubstituted α-oligothiophenes[12−18] and other π-conjugated compounds.[35,36] Molecules are aligned with their longer molecular axis parallel to one another and inclined from the lattice plane (b−c plane). This feature, together with lattice parameters (monoclinic, $a =$ 22.447 Å, $b = 7.716$ Å, $c = 5.992$ Å, $\beta = 91.43°$, $Z = 2$) are close to those of the low-temperature phase of α-6T (monoclinic, $a = 44.708$ Å, $b = 7.851$ Å, $c = 6.029$ Å, $\beta =$ 90.76°, $Z = 4$).[15]

On the other hand, β5T exhibited a different packing manner (Figure 2b). The molecular long axis is almost perpendicular to the lattice plane (a−c plane). Such a packing is seldom and has been reported for some thiophene-phenylene co-oligomers by Hotta et al.[37,38] According to their investigation, a compound with its molecular long axis bent at the middle (i.e, a compound with C_v symmetry) tends to show the perpendicular orientation.

Band Structure Calculation. Band structure calculation out of single-crystal structure data provides intrinsic electronic property of molecular materials and is thus informative for molecular design. Since oligothiophenes often function as a p-type semiconductor (hole carrier), we focused on the HOMO bands (Figure 3). 0 eV of the vertical axis corresponds to the HOMO energy level of an isolated molecule. The horizontal axes of each diagram are taken so that the herringbone geometries of the two compounds are comparable; i.e., the band structure of the right-hand side of each diagram corresponds to the packing direction where the herringbone angles are smaller than 90° (more $\pi-\pi$ overlap).

β6T exhibits large dispersion at Γ, exhibiting well-developed two-dimensional band structure. The feature of

(35) Enkelmann, V. In *Handbook of Oligo- and Polythiophenes*; Müllen, K., Wegner, G., Ed.; Wiley-VCH: New York, 1998; Chapter 5.
(36) Curtis, M. D.; Cao, J.; Kampf, J. W. *J. Am. Chem. Soc*. **2004**, *126*, 4318.
(37) Hotta, S.; Goto, M. *Adv. Mater*. **2002**, *14*, 498.
(38) Hotta, S.; Goto, M.; Azumi, R.; Inoue, M.; Ichikawa, M.; Taniguchi, Y. *Chem. Mater*. **2004**, *16*, 237.

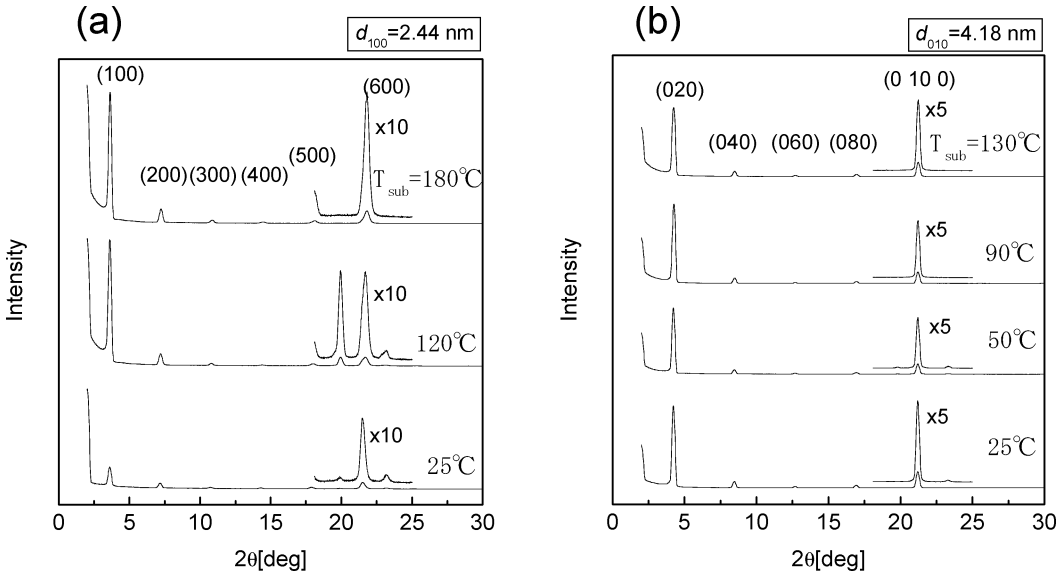

Figure 4. X-ray diffraction patterns of (a) β6T and (b) β5T films (thickness of ca. 100 nm) fabricated at various substrate temperatures (T_{sub}).

the band is similar to that of α4T[13] and α6T.[16] The largest bandwidth is calculated to be 0.054 eV. On the other hand, β5T exhibits more complicated structure because of the existence of four molecules in a two-dimensional asymmetric unit cell. The band is split into four and displays two pairs with a gap in between. The largest bandwidth is calculated to be 0.052 eV between the highest and the lowest levels and 0.027 eV between the highest and the second highest levels. The larger value of β6T over those of β5T suggests the more enhanced hole mobility of β6T.

Molecular Packing in Thin Films. Figure 4 shows the XRD patterns of β6T and β5T films deposited at various substrate temperatures. In the XRD results of β6T (Figure 4a), diffractions corresponding to the (h 0 0) plane of a single crystal were observed up to the sixth. In the case of β5T film (Figure 4b), diffractions corresponding to the (0 k 0) plane of a single crystal were observed up to the tenth (even number only). These results indicate the well-ordered and layer-by-layer film growth, where the molecular long axis standing perpendicularly on the substrate. The d-spacing of the (h 0 0) plane in the β6T film and (0 k 0) plane in the β5T film are calculated to be d_{100} = 2.44 nm and d_{010} = 4.18 nm, respectively. The positions of (h 0 0) peaks for β6T and (0 k 0) peaks for β5T did not depend on the substrate temperature. In both films, weak diffraction peaks were observed at around $2\theta = 20°$ and 23°. Based on the indexing of simulated powder diffraction patterns using single-crystal analysis results (see Supporting Information), these peaks are assigned to be the diffraction originating from crystal domains with different orientations in which molecular long axis lies on the substrate. The above shows the existence of crystalline domains in which the molecular long axis lies on the substrate, although their small intensity indicates that such crystalline portion is small.

In the case of β6T films, the larger diffraction intensity of (h 0 0) was obtained for the film fabricated with higher substrate temperature. In other words, high substrate temperature induces a highly crystallized film. The d-spacing of the (h 0 0) plane in the β6T film (d_{100} = 2.44 nm) is larger than that of a single crystal (d_{100} = 2.24 nm), indicating the existence of a different polymorph with the molecular long axis standing on the molecular layer more vertically compared with that of a single crystal.

On the other hand, intensities of (0 k 0) diffraction of β5T films were independent of the substrate temperature. It means that highly crystallized films are deposited even at low substrate temperature. The d-spacing of the (0 k 0) plane in the β5T film (d_{010} = 4.18 nm) equals that of β5T single crystal. Therefore, β5T film exhibits the same polymorph as that of a single crystal, with the molecular long axis standing perpendicularly on a molecular layer and a substrate.

Film Morphology. Figure 5 shows the AFM images of β6T and β5T films deposited at various substrate temperatures. Flat, well-developed platelet domains were observed for all the images except for the case of the films prepared at 25 °C (Figures 5a and 5d). Such flat domains have often been observed for the evaporated films of small molecules with highly anisotropic shape, where their molecular long axis tends to stand with respect to the film surface.[4,12,24−26,39,40] The AFM observations for β6T and β5T films are therefore consistent with the above-mentioned XRD results with dominant sequential peaks corresponding to the d-spacing of the molecular long axis.

When the substrate temperature was increased, the grain sizes of β6T and β5T films grew larger. In the images of the films prepared at excessively high substrate temperature (β6T: 180 °C; β5T: 130 °C), large grain boundaries and cracks were observed. Similar correlation of film morphology and substrate temperature has been reported for other organic materials such as α-oligothiophenes[22−24] and pentacene.[39,40] Apart from the platelet domains, needle-like crystals coexist in the films prepared under certain conditions. Since the minor XRD peaks at around $2\theta = 20°$ and 23° were observed only for the films that contain the needle-

(39) Shtein, M.; Mapel, J.; Benziger, J. B.; Forrest, S. R. *Appl. Phys. Lett.* **2002**, *81*, 268.
(40) Dimitrakopoulos, C. D.; Brown, A. R.; Pomp, A. *J. Appl. Phys.* **1996**, *80*, 2501.

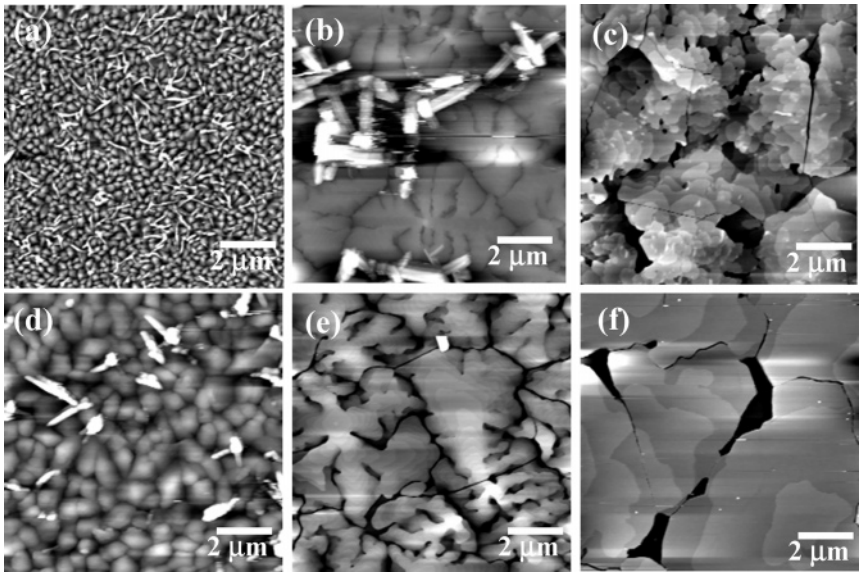

Figure 5. AFM images (10 μm × 10 μm) of films (thickness of ca. 100 nm) fabricated at various substrate temperatures. (a) β6T, fabricated at 25 °C; (b) β6T, fabricated at 120 °C; (c) β6T, fabricated at 180 °C; (d) β5T, fabricated at 25 °C; (e) β5T, fabricated at 90 °C; (f) β5T, fabricated at 130 °C.

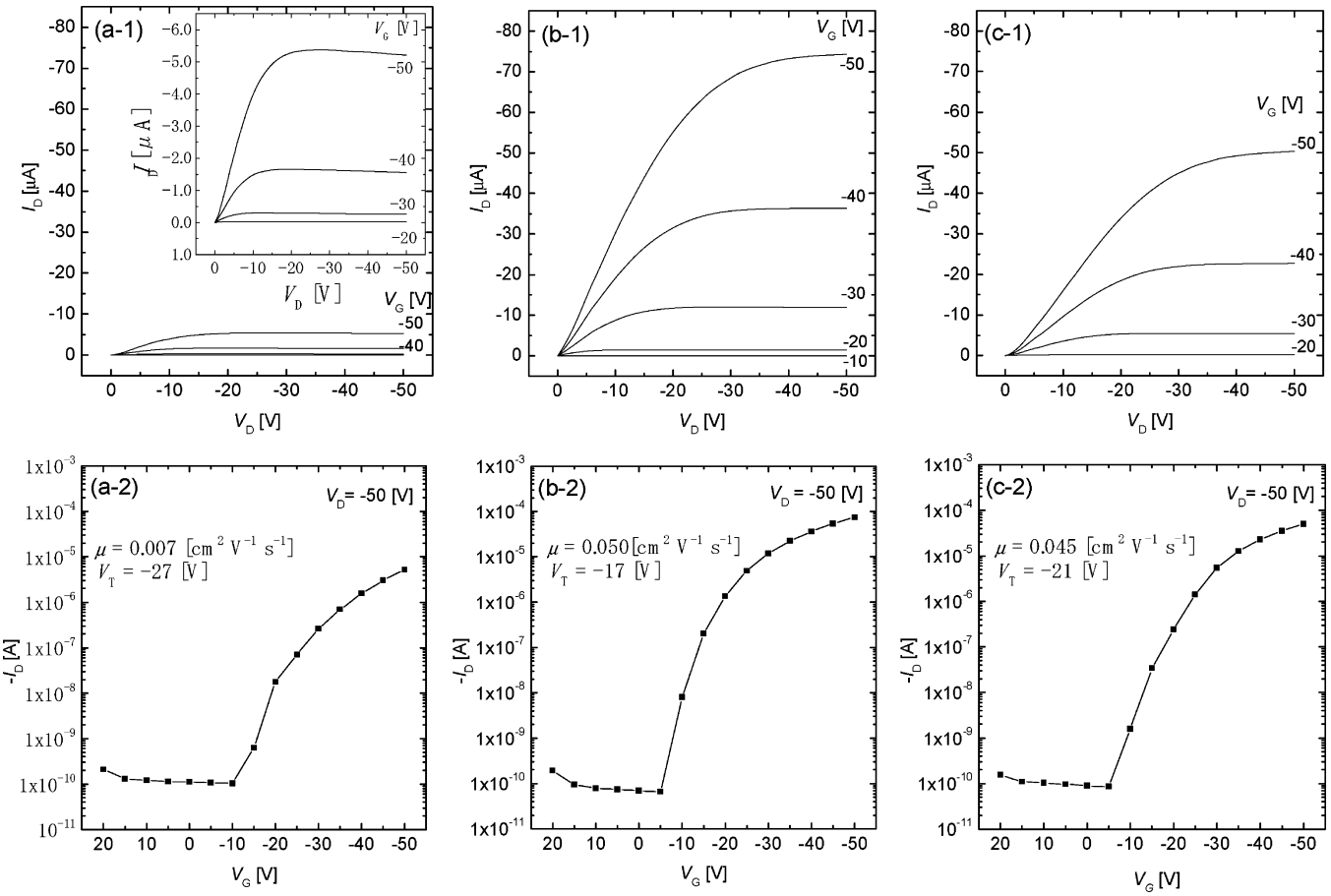

Figure 6. OFET characteristics of β6T films fabricated at various substrate temperatures: (a) 25 °C; (b) 120 °C; (c) 180 °C. The inset of (a-1) represents the magnification.

like crystals, these minor crystalline domains are deduced to be the domains where the long molecular axis lies flat on the film surface.

Field-Effect Transistor Characteristics. Figures 6 and 7 show the OFET characteristics of β6T and β5T films fabricated at various substrate temperatures, respectively. All the films exhibited p-type characteristics whose mobility values are within 7×10^{-3} to 5×10^{-2} cm^2 V^{-1} s^{-1}. The I_d-V_d curves show well-expressed plateau (saturation regime) at high drain voltage region and a strong increase of the drain current with increasing gate voltage. Table 2 shows the summary of OFET properties of β6T and β5T films fabricated at various substrate temperatures. For comparison, OFET properties of pentamer, hexamer, and heptamer of

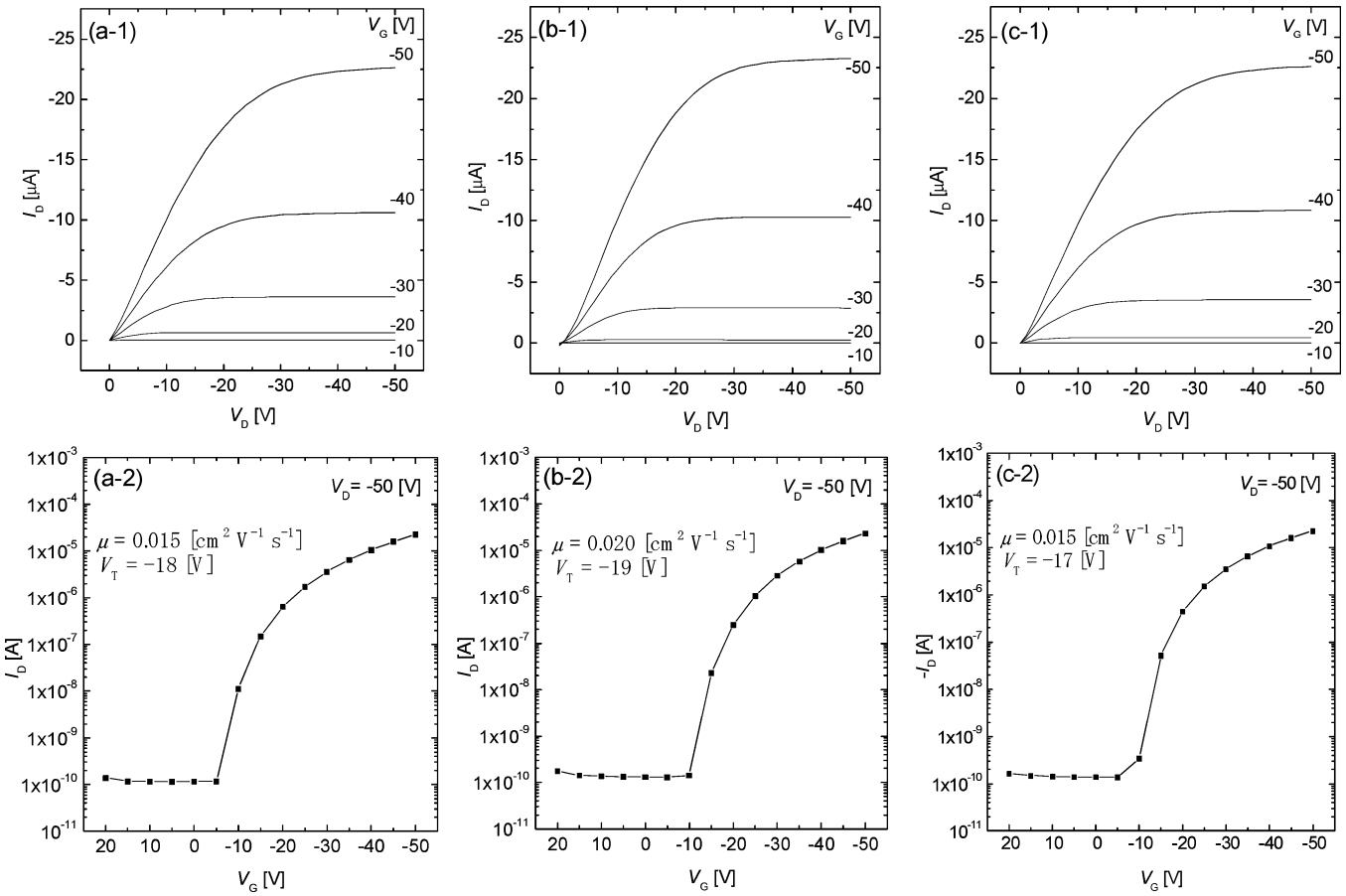

Figure 7. OFET characteristics of β5T films fabricated at various substrate temperatures: (a) 25 °C; (b) 90 °C; (c) 130 °C.

Table 2. Field-Effect Mobility, Threshold Voltage, and On−Off Ratio of OFETS Based on Oligothiophene Films

compound	substrate temperature [°C]	field-effect mobility (μ) [cm^2 V^{-1} s^{-1}]	threshold voltage (V_T) [V]	on-off ratio (I_{ON}/I_{OFF})
β6T (this work)	25	0.007	−27	10^5
	120	0.050	−17	10^5
	180	0.045	−21	10^5
β5T (this work)	25	0.015	−18	10^5
	50	0.015	−20	10^5
	90	0.020	−19	10^5
	130	0.015	−17	10^5
α7T[22]	200	0.13		
α6T[22]	120	0.08		
α5T[22]	90	0.05		

α-oligothiophene (α*n*T; $n = 5, 6, 7$) films fabricated at high substrate temperature[22] are also shown in Table 2. Both β6T and β5T show smaller values of hole mobility compared with their α*n*T isomers.

OFET characteristics of β6T film depended on the substrate temperature (Figure 6). The OFET fabricated at 25 °C showed mobility $\mu = 0.007$ cm^2 V^{-1} s^{-1} and threshold voltage $V_T = -27$ V. OFET fabricated at 120 °C exhibited improved property: $\mu = 0.050$ cm^2 V^{-1} s^{-1} and $V_T = -17$ V. Together with the XRD and AFM observations, it can be deduced that better crystallinity and larger grains of the film prepared at higher temperature enable faster carrier transport. Similar phenomena have been reported for thin films of other organic semiconductors such as α-oligothiophenes[21−24] and pentacene.[39] OFET properties at a substrate temperature of 180 °C were worse compared with that at 120 °C: the values are $\mu = 0.045$ cm^2 V^{-1} s^{-1} and $V_T = -21$ V. The results indicate that grain boundaries and cracks caused by excessively high substrate temperature block the carrier transport in the film.

In the case of β5T, OFET characteristics did not depend much on the substrate temperature despite the difference in film morphology depending on the substrate temperature (Figure 7). The optimized mobility value of 0.020 cm^2 V^{-1} s^{-1} was obtained at a substrate temperature of 90 °C where large grains were observed. The deviation of mobility, however, is not very large: the mobility is 0.015 cm^2 V^{-1} s^{-1} at 25 and 50 °C where grains are small and 0.015 cm^2 V^{-1} s^{-1} at 180 °C where large grains were observed.

Usually, film morphology strongly affects OFET performance, while β5T film is not the case. We consider that the uncommon crystal structure of β5T results in the independence on the film morphology. The metastable polymorph observed for β6T film may prevent the formation of highly crystallized film. Moreover, boundaries of domains in which the azimuthal direction of the molecular long axis is different from one another (Figure 8a) may impede the carrier transport. In contrast, β5T films show the same polymorph as that in a single crystal with the long molecular axis standing perpendicularly on the substrate. In other words, β5T films can grow in a thermodynamically stable state, which is advantageous for the growth of a highly crystallized film. Moreover, the long molecular axis exhibits complete uniaxial orientation, which may enable the smooth carrier transport at grain boundaries (Figure 8b).

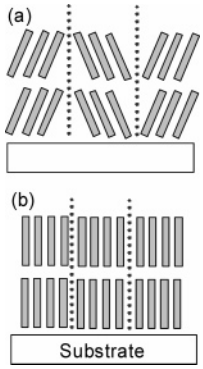

Figure 8. Grain boundary models of (a) β6T and (b) β5T.

Conclusion

Using unsubstituted oligothiophene pentamer and hexamer with both terminal thiophene units linking at the β-position (β*n*T; $n = 5, 6$), we have investigated the relationship between molecular structure, molecular packing in bulk, film structure, and electrical characteristics using X-ray single-crystal analysis, XRD, AFM, and OFET fabrication and characterization. X-ray single-crystal analysis revealed uncommon molecular packing geometry of β5T where the molecular long axis is almost perpendicular to the lattice plane (a−c plane). On the other hand, β6T shows common molecular packing geometry that is often observed for many rodlike organic semiconducting molecules such as pentacene and α-oligothiophenes. β5T films grow up while maintaining the same crystal structure as a single crystal, while the β6T films grow up in an original crystal phase. β6T and β5T function as p-type organic semiconductors. Highest field-effect mobility of OFET was 0.050 $cm^2\ V^{-1}\ s^{-1}$ for β6T at a substrate temperature of 120 °C and 0.020 $cm^2\ V^{-1}\ s^{-1}$ for β5T at a substrate temperature of 90 °C. The OFET characteristics of β6T depended on the substrate temperature, while those of β5T were independent of the substrate temperature. It can be considered that such a feature of β5T originates in its uncommon crystal structure.

Acknowledgment. We thank Professor Takehiko Mori of Tokyo Institute of Technology and Dr. Hisashi Tanaka of AIST for their helpful suggestions on band structure calculations.

Supporting Information Available: Crystallographic information in CIF format; simulated powder XRD patterns. This material is available free of charge via the Internet at http://pubs.acs.org.

CM0701658